Characterization of the Flight CCD Detectors for the GOES N and O Solar X-ray Imagers

Robert A. Stern[a], Lawrence Shing[a], Paul Catura[a], Mons Morrison[a], Dexter Duncan[a], James R. Lemen[a], Tim Eaton[b], Peter Pool[b], Roy Steward[b], Dave Walton[c], Alan Smith[c]

[a]Lockheed Martin Solar and Astrophysics Laboratory,
Dept. L9-41, Bldg. 252, 3251 Hanover Street, Palo Alto, CA 94304, USA

[b]e2v technologies, Waterhouse Lane, Chelmsford, Essex CM12QU, UK

[c]Mullard Space Science Laboratory, Holmbury St. Mary, Dorking, Surrey RH5 6NT,UK

ABSTRACT

A new Solar X-ray Imager (SXI) using back-illuminated, anti-blooming CCD technology will become part of the instrument complement on NOAA's GOES (Geosynchronous Orbiting Environmental Satellite) N and O spacecraft, with probable launch dates beginning in the 2004-2005 time frame. SXI N and O were developed under a NASA contract by the Solar and Astrophysics Laboratory at the Lockheed Martin Advanced Technology Center, and are currently being integrated into their respective spacecrafts by Boeing Space Systems. SXI N and O will each provide full disk images of the Sun from 0.2 to 1.2 keV (10–60 Å) through the combination of a grazing incidence telescope, bandpass filters, and an X-ray imaging CCD. The custom designed, back-illuminated CCDs were fabricated and initially tested by Marconi Technologies (formerly EEV Ltd, now e2v technologies), screened in visible light by the Mullard Space Science Laboratory, and fully characterized in both visible light and X-rays at LMSAL. By minimizing the field-free region within the CCD, the spatial resolution at low X-ray energies was significantly improved. The SXI CCDs also exhibit only very modest response changes as a result of solar X-ray exposure, based upon extended life tests. The flight CCDs meet or surpass all specifications for quantum efficiency (QE), spatial uniformity, defects, charge transfer efficiency, QE stability in vacuum, read noise, linearity, full well and dark current. A QE model based on earlier work with ion-implanted, laser-annealed CCDs provides a consistent picture of the CCD response from soft X-rays through far UV wavelengths.

Keywords: back-illuminated CCD, Solar X-ray Imager (SXI), X-rays, CCD characterization

1. INTRODUCTION

In a broad-based effort to better understand and predict space weather, NOAA, NASA, and the USAF began a program to provide near-continuous imaging of the solar corona in soft X-rays from the GOES (Geosynchronous Operational Environmental Satellite) spacecraft. The first Solar X-ray Imager (SXI), developed by the NASA Marshall Spaceflight Center, is currently operating on the GOES-12 spacecraft.[1,2] The GOES-12 SXI instrument uses a combination of Ni-coated, Wolter I grazing incidence optics and a microchannelplate intensifier/phosphor system fiber-optically coupled to a CCD working at visible wavelengths.

Subsequent SXI instruments will be flown on GOES N and O, beginning in 2004-2005. The Lockheed Martin Solar and Astrophysics Laboratory (LMSAL) at the LM Advanced Technology Center (LMATC), designed and built SXI N and O. The new SXI instruments use an uncoated Zerodur grazing incidence X-ray telescope with an optical prescription[3] optimized for a wide (42′) FOV in conjunction with a dual filter wheel, rotary shutter, and a back-illuminated, direct imaging X-ray CCD. The overall characteristics of the SXI N and O instruments are described elsewhere in these proceedings.[4] The CCDs for SXI N and O were provided by EEV/Marconi Ltd (currently e2v technologies) to the Mullard Space Science Laboratory (MSSL) for initial testing, and subsequently to LMSAL for final screening and X-ray characterization. In an earlier paper, we described preliminary testing of evaluation CCDs[5]; in this paper, we discuss the results of spatial resolution and extended life testing on the evaluation CCDs and the visible and X-ray characterization of the flight CCDs. Details of the LMSAL experimental apparatus (X-ray sources, Talktronics camera system, vacuum chambers) can be found in our earlier paper.[5]

Further author information: E-mail: stern@lmsal.com

Telescopes and Instrumentation for Solar Astrophysics, edited by Silvano Fineschi, Mark A. Gummin,
Proceedings of SPIE Vol. 5171 (SPIE, Bellingham, WA, 2004) · 0277-786X/04/$15 · doi: 10.1117/12.506346

Figure 1. CCD64 in SXI O Focal Plane. Two integrated circuit temperature sensors are mounted above and below the shiny (back-illuminated) CCD surface.

TEST PURPOSE	TEST TYPE
Basic Device Parameters	LTC Fe 55 Gain and CTE Dark Current
X-Ray Quantum Efficiency	QE (Cu L, O K, C K, B K, Be K, Si L, Al L)
Device Response Uniformity	Flat Field (Blue and Green LEDs, C K, Cu L, Al K)
Spatial Resolution	Single-Photon MCC (Cu L, Al K, Fe 55)
Lifetime softer Solar X-rays	High Dose (C K)
Lifetime harder Solar X-rays	High Dose (Al K)

Figure 2. CCD Evaluation test matrix. Shaded boxes indicate key discriminators for SXI instrument. LTC = Light Transfer Curve, MCC = Mean Charge Capture (see text)

2. FLIGHT SXI CCD DESIGN

The SXI CCD design (CCD64) is a full frame imager, with 16 μm (5 arc-sec) pixels in a 512×580 (N-S vs E-W projected on the solar disk) array.[5] A shielded-drain anti-blooming structure is provided to limit charge spillage under high signal overload conditions (blooming) while maximizing the quantum efficiency for back-illuminated operation. The devices are ion-implanted and laser annealed to produce an electrical barrier to charge recombination at the back surface. The back surface of the CCD is further passivated to optimize the X-ray response for low energy ($\lesssim$500eV or $\gtrsim$25 Å) photons. The CCD is housed in a rugged tungsten-copper and ceramic package (Fig. 1) and is provided with three reference fixing lugs for accurate mechanical mounting.

3. CCD DESIGN OPTIMIZATION

Apart from the basic CCD64 design, which was largely dictated by the SXI requirements, early concerns included long term effects of solar X-ray exposure on the CCD response, soft X-ray quantum efficiency (QE), and the effects of charge diffusion on the spatial response of the CCD. To address these issues, a cooperative effort among LMSAL, MSSL and e2v technologies was conducted with the support of NASA and NOAA. This evaluation program was structured such that two batches (20 and 100 Ω-cm resistivities) of CCD wafers were produced, with variations in backside treatments applied to each batch.[5] The resulting CCD64 "flavors" (100 Ω-cm "Basic", "Enhanced" and "GILD" and 20 Ω-cm "Enhanced"- see Ref. 5) were then evaluated using the criteria shown in Figure 2 at e2v technologies, MSSL and LMSAL prior to selecting the optimum devices for SXI. Sufficient wafers from each batch were held in reserve for production of flight devices, once the decision to proceed with a particular resistivity and backside process was made.

In general, we found only modest performance differences among the CCD "flavors": as might be expected, all behaved rather similarly with respect to parameters such as full well, charge transfer efficiency (CTE), on-chip amplifier gain, dark current, read noise, etc. Devices with the "Basic" and "GILD" backside treatments showed somewhat (25-40 %) lower effective QE at E < 0.25 keV (λ > 45 Å); however, our SXI instrument design had sufficient margin at soft energies that even these devices would have met the SXI QE requirements. Of the

remaining criteria, the two most important were the long term effects of exposure to solar soft X-rays and spatial resolution performance.

3.1. Effects of Long Term Solar X-ray Exposure

Because of past experience with severe degradation in back-illuminated CCDs produced by SITe for the Extreme Ultraviolet Imager (EIT) on SOHO,[6] we were initially very concerned about similar effects during the 5 year operational lifetime of SXI. To examine such effects, we conducted life tests at two X-ray energies: 0.28 and 1.5 keV (C K 44.7 and Al K 8.34 Å). The 0.28 keV X-rays are absorbed very close to the back-illuminated CCD surface (1/e depth ~ 0.1 μm), while the 1.5 keV X-rays penetrate much deeper (~ 8 μm), with a significant flux reaching the front circuitry of the CCD in the case of the 20 Ω-cm (~ 8 μm thick) CCDs. For both tests, a small fraction of the CCD was illuminated through a circular or half-circular aperture using a high intensity X-ray beam. The total integrated X-ray dose corresponded to a substantial fraction of the expected exposure over an entire mission (the beam spectrum was periodically monitored using a proportional counter to ensure that the flux was primarily the characteristic K radiation from the C or Al targets). As the exposure was accumulated, the aperture was temporarily removed, and dark images, X-ray and blue (430 nm) "flat fields" were taken. The differences in the CCD dark current and response between the exposed and unexposed areas were then measured.

The results from the C K tests on several devices with the "Enhanced" and "GILD" backside treatments showed a gradual decrease in CCD sensitivity (see Figure 3); however, the predicted effect over the course of the 5 year mission ($\sim \sim 2.8 \times 10^6$ exposures) is estimated to be $\lesssim$15-20 %. The response change can be significantly mitigated through regular annealing of the CCD at room temperature (as shown in the bottom plot of Figure 3), and in fact is likely to be even less than predicted, since our test was conducted over an accelerated time period (~ 2 weeks). This result gave us confidence that use of the "Enhanced" backside process would not be of concern regarding long term solar exposure, and that the use of the "GILD" process (which does not involve an ion implant, hence should not produce significant back surface trapping) would not provide substantially better performance.

In contrast, lifetime tests using the more penetrating Al K soft X-rays were designed to test effects on the frontside circuitry. The combination mirror material (Zerodur) and graze angle will prevent hard X-rays from reaching the CCD; however, photons with energies up to ~ 1 keV (12 Å) will be reflected by the SXI optics. Despite a 1/e attenuation length ~ 2.7 μm, some fraction of these X-rays can penetrate the thin (8 μm) substrate to reach the oxide layers. We note that use of a back-illuminated device provides significant protection for softer X-rays compared to a front-illuminated CCD, in which only the much thinner (sub-μm) gate structures shield the CCD oxide layer. Estimates of the expected ionizing dose in the SXI CCD gates is dependent upon actual SXI operations, and the fraction of the solar disk covered by active regions and coronal holes (as well as flares). An initial estimate suggests a range of $\sim$ 5–35 kRad: we decided to test the imaging area of a non-flight SXI CCD to the upper limit of this range using the Al K source. We found that most of the properties of the CCD were unaffected by this dose, except for an $\sim$2 increase in the CCD dark current, which is most likely the result of trapped charge in the CCD oxide layers. We note that, unlike other forms of radiation damage from high energy particles, the CCD serial registers and output node will not be affected by such damage, only the imaging portion of the array. Based upon shielding models, we expect that the ionizing dose level will be $\lesssim$3 kRad from other radiation sources in orbit.

3.2. Effects of Charge Diffusion on Spatial Resolution

Another important concern for the SXI flight CCDs is the effect on spatial resolution of charge diffusion in the CCD pixels. Although back-illuminated CCDs have significantly better QE in soft X-rays than front illuminated devices (see, e.g. results from the CHANDRA ACIS devices[7]), they do suffer the effects of "charge spreading" to adjacent pixels more than front illuminated devices at lower energy X-ray energies. This is primarily because electrons created near the back surface of the CCD, in a relatively "field free" region, may experience significant charge diffusion before drifting under the influence of the CCD gate potential and accumulating in the CCD wells. The amount of "charge spreading" depends upon a number of factors, including photon energy, CCD resistivity, device thickness, and gate potential. In an integrating CCD, such as for the SXI, the result of such charge spreading is a degradation in image resolution. Since the CCD pixel size determines the sampling of this charge

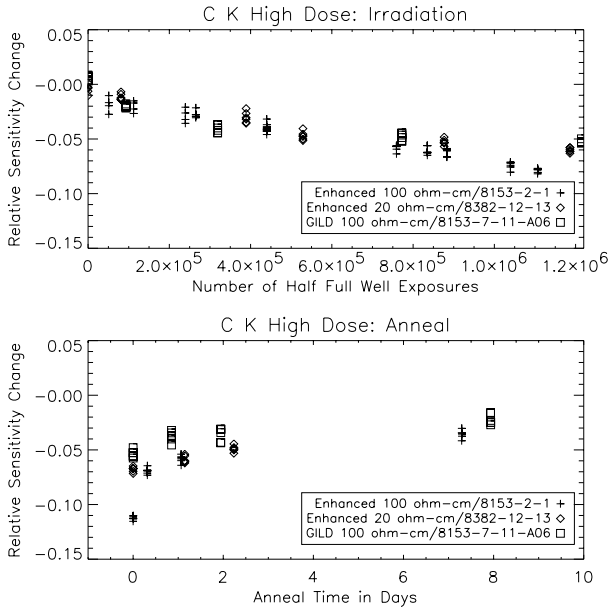

Figure 3. C K Irradiation and anneal tests. Top: drop in C K response vs. number of equivalent 50% of full well exposures. A total of 1.1×10^6 exposures corresponds to $\sim 40\%$ of mission life, assuming one exposure/minute for 5 years. The upturn at the right side of the figure represents an unintended "anneal". Bottom: the change in response after the high dose X-rays are stopped, the devices are warmed to room temperature without breaking vacuum and periodically re-cooled to take X-ray flats.

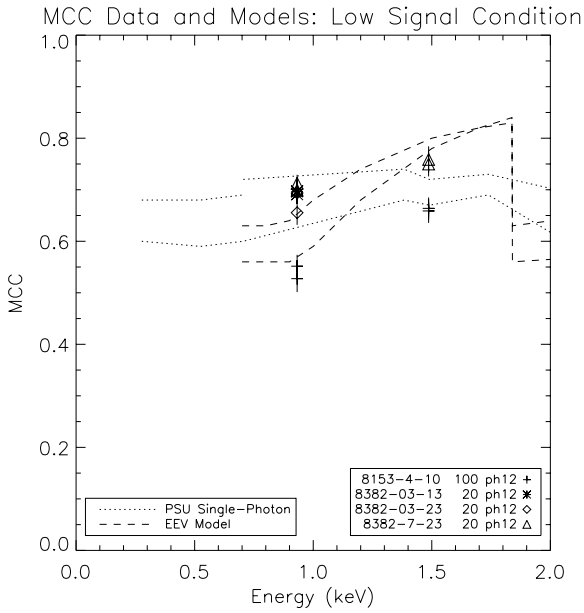

Figure 4. MCC Results. Measured MCC values for three "thin" (20 Ω-cm, batch 8382) devices and one "thick" (100 Ω-cm, batch 8153) device are shown. The "ph12" labels refer to the fact that two of the three parallel clock phases were help high during integration, as is the case for flight operation. The two models are described in the text.

spreading, the effects on the overall instrument spatial response will also depend upon the level of sampling the telescope point response, and the relative sizes of the telescope and CCD image point spread function (PSF). In the case of the on-axis response of the SXI instrument, the CCD does contribute a non-negligible amount to the overall PSF.[4] Thus a significant part of our optimization program involved both measuring and modelling the effects of charge diffusion in candidate SXI CCDs.

Our approach was to select a figure-of-merit that was easily measurable, which we termed Mean Charge Capture (MCC). We defined this as the fraction of charge from each photon event retained in the central pixel for a uniformly illuminated CCD (for a given photon event in which charge diffuses to adjacent pixels, the central pixel was assumed to be the one with the largest level of charge). To measure this quantity, we found that the simplest approach was to operate the CCD in single-photon counting mode using either a radioactive source (^{55}Fe - 5.9 keV) or a low intensity X-ray beam (at Cu L - 0.93 keV and Al K - 1.5 keV). Exposure times were chosen to insure that photon events were clearly separable on the CCD image (with the occasional multiple event subsequently removed via software).

For a succession of 30 or more images, we extracted a 5x5 pixel region surrounding the peak pixel in each event, summed the resulting charge, and calculated the fraction of total charge in each pixel. Since X-ray photons were initially absorbed at random locations within each pixel, accumulation of several thousand or more events at each energy then allowed us to determine the MCC parameter. To ensure that no significant amount of charge was diffusing to larger regions, we calculated the total average charge collected for all events and compared it to the expected amount of charge, based upon the photon energy and the charge collection efficiency model of the CCD (see § 5.1). We then compared our results to two sets of models: one computed by e2v technologies based upon an analytical approximation to the CCD characteristics, and another a semi-empirical model based upon Monte Carlo calculations developed at Penn State for analysis of Chandra ACIS CCD charge transfer

inefficiency.[8] The CCDs tested were "Enhanced" devices with significant differences in the amount of field free region and overall thickness, either: (a) 20 Ω-cm resistivity, $\sim 8\mu$m thick, or (b) 100 Ω-cm resistivity, $\sim 15\mu$m thick. The results of our testing compared to the two models are shown in Figure 4. As a result of these tests, it was determined that the improvement of the MCC at 0.93 keV from ~ 0.55 to 0.70 was of sufficient importance to the overall instrument performance that the thinner, 20 Ω-cm resistivity device was adopted for the flight CCDs.

In addition, we performed a test designed to replicate charge diffusion effects for images exposed to a significant fraction of the CCD pixel full well. The depletion region in a CCD pixel decreases as charge accumulates (i.e. the depth of the "field-free" region in a CCD *increases*); charge spreading – and thus spatial resolution – is expected to worsen for such images. We mimicked this effect through a series of single-photon MCC experiments carried out with differing gate voltages on the CCD pixel (varying the depletion depth/field-free region). These latter tests confirmed the superior spatial response of the lower resistivity, thin devices, and will enable us in the future to better model the spatial response of the SXI at high signal levels characteristic of solar X-ray observations.

4. FLIGHT DEVICE SCREENING

After determination of the optimal CCD characteristics (20 Ω-cm, "Enhanced" backside process), we began screening and characterizing flight candidate devices. The devices were selected from among several CCD64 wafers in a single batch, based upon number of defects, full well capacity, read noise, dark current, and other characteristics prior to final packaging. Among other steps, the devices were subjected to electrical "burn-in" and thermal cycling designed to weed out devices prone to failure in the relatively severe space environment. After inspection and visible light characterization at e2v technologies, the flight CCDs were delivered to MSSL, where they underwent initial flat field screening in visible light. This process weeded out a handful of devices with undesirable variations in visible flat field response, especially at blue ($\sim$ 430 nm) wavelengths, which because of the short absorption depth at these wavelengths of ~ 0.1 μm, indicates potential problems at soft X-ray energies (e.g. C K). The 20 flight devices which met our requirements were then shipped to LMSAL, in addition to a similar number of non-flight devices (in flight packages) that were reserved for other uses.

4.1. LMSAL Screening System

The characteristics of the flight devices were such that any of them could meet the requirements of the SXI instrument. Based upon earlier results from evaluation CCDs, we expected that their X-ray performance would be similar. However, X-ray characterization and calibration is relatively time consuming; thus we selected a small number of devices with the fewest point defects (flight devices were required to have zero bad columns), lowest dark current, etc. for final X-ray calibration. This screening process required a semi-automated approach in order to maintain uniformity of the test results, and reduce the manpower required to characterize the flight devices.

To this end, we assembled a separate screening system, using a duplicate cold head and Talktronics camera system. The cold head was installed in a previously constructed low contamination turbopumped vacuum system capable of reaching $\sim 10^{-7}$ torr with negligible contamination from organic compunds.[9] It consists of a windowed port connected to the vacuum chamber, connected to a vacuum cross which included an insertable ^{55}Fe source, and a through port to a shutterable and selectable (blue, green, red) LED source used to provide flat field illumination of the CCD. For such flat fields, a diffuser was manually inserted in front of the CCD.

4.2. Camera Software and Test procedure

To provide a standard set of test images for all devices, we developed camera sequencing software which, once the screening system source (and optionally, diffuser) was properly configured, would automatically take the proper series of exposures. For example, to determine the system gain by the traditional "light transfer" curve, pairs of exposures (and a corresponding dark frame) were taken with one of the LEDs at a series of different exposure times. This set of images also served to determine the CCD plus test system linearity. ^{55}Fe frames were taken to determine charge transfer efficiency (CTE), and flat fields were taken with blue and green LEDs to determine overall uniformity and also topinpoint individual pixel defects. These data were taken at temperatures of -80 C to +20 C, at 20 C intervals (some frames, e.g. ^{55}Fe, were omitted at the the higher temperatures, where the

dark current limits the ability to detect single photon events). A graphical interface using IDL was developed, which allowed the test operator to enter basic CCD information (CCD type, serial number, etc.) using a series of prior templates, and start a preprogrammed sequence (or series of sequences) using a selectable menu and mouse clicks.

The camera software also wrote extensive information to a data header structure for each CCD frame, which was later incorporated into the header of a FITs image. The standardization of the header information was critical to later, automated analysis of the screening data. For each CCD, the screening data involved taking roughly a few hundred images over the course of a day: much of the time was spent cooling down the CCD to successively lower temperatures and waiting for temperature to stabilize to within ~ 0.1 C before beginning the next set of images. As the FITs images were taken, they were transferred via local network to our laboratory UNIX-based workstation; the test operator also kept a text log file indicating the times of data taking and any anomalies in the procedure.

4.3. Analysis Software

To provide a uniform analysis of the screening data, a UNIX shell script and IDL procedures were written. A single command line used as a parameter the file directory (or directories) in which the FITs screening files for a given CCD were kept. Invocation of this command line began an IDL batch job which accumulated the FITs headers for all files, searched them for specific preset image sequences, and subsequently processed each sequence in turn, checking for anomalies such as unusually large temperature variations, incorrect source configurations, missed frames, etc. In such cases, the sequence was rejected and the frames not processed. The analysis included system gain (using several methods), flat fields, CTE, camera/CCD linearity (Talktronics lab system only), dark current as a function of temperature, system noise, etc. The results of this analysis were output in both text and graphical forms, and archived as a variant of an IDL save file ("*.geny") used by the Solar Soft IDL library.[10] This allowed for re-analysis of the image data at a later time as the software was improved or corrected.

4.4. Results

As a sample of the batch analysis results, we show in Figures 5, 6, 7, and 8 graphical outputs from the defect mapping, ^{55}Fe event "dotplots" for determination of charge CTE, system gain comparisons as a function of temperature, and system non-linearity (CCD + Talktronics). The results shown in these figures are fairly representative of the flight CCDs, which we found to be very similar in their properties (which might be expected, considering they came from only one or two wafers of a single batch). In the case of the flat field images, only a handful of defects were found to be $> 10\%$; the residual variation of $\lesssim 1\%$ (diagonal striping) in CCD flat-field response was primarily the result of the laser anneal process. The ^{55}Fe CTE measurements all indicated CTI (Charge Transfer Inefficiency = 1.0 – CTE)$< 1 \times 10^{-5}$. Gains measured by a two-frame light transfer technique,[11] a multiple-frame light transfer technique, and the ^{55}Fe Kα peak all agreed to within $\sim 5\%$ (^{55}Fe measurements required T < -40 C); non-linearity was generally $< 1\%$.

5. X-RAY CHARACTERIZATION

As a result of the screening process described in the previous section, a small number of devices were selected for final X-ray characterization and QE calibration. These measurements were carried out using the LMSAL XUV calibration system[12] using the same procedures and analysis techniques as discussed in our previous paper.[5] Although the normal operating range of SXI is ~ 0.2–1.2 keV (10-60 Å), we also took EUV and UV measurements on one CCD to help constrain the model parameters.

5.1. QE Measurements and Modeling

The results of our QE measurements and modelling for five SXI flight CCDs are shown in Figure 9. e2v technologies provided information on the detailed implant profile in the SXI CCDs, and we based our modelling on the formal solutions of CCD charge collection efficiency described in earlier work on ion-implanted, laser-annealed CCDs.[13] Using these solutions involved fixing the estimated back surface native oxide thickness, and the device overall thickness (the latter parameter has little effect on the solution because of the low energy of the X-rays studied). The effect of assuming differing levels of surface recombination efficiency (S) is seen in

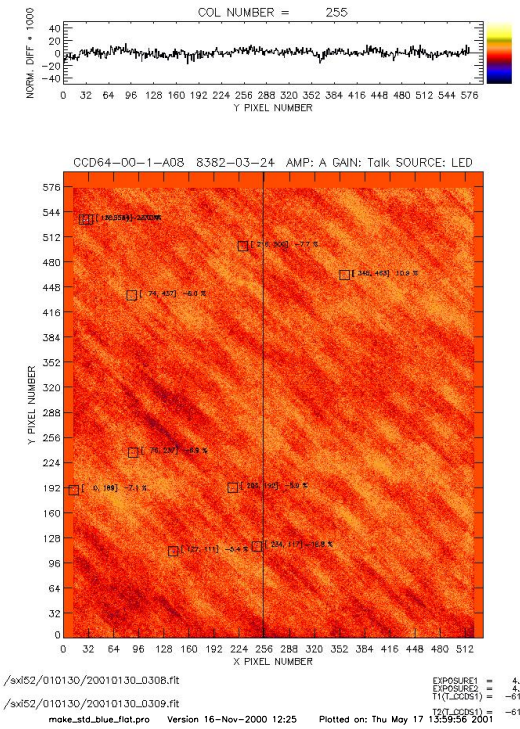

Figure 5. Blue (430 nm) LED flat field and defect map. The flat field is generated by fitting a 4th-order polynomial to the raw diffuse LED illumination, and a difference image is created by subtracted the fitted smooth polynomial from the raw data and dividing the difference by the fitted data. The scale in the upper line plot is in units of parts per 1000: i.e. the scale is ±5%. Individual defects (all black) > 5% are indicated by labelled boxes on the image. The vertical dark line in the image is *not* a column defect, but is drawn by software to indicate the vertical cut displayed in the upper figure as a line plot.

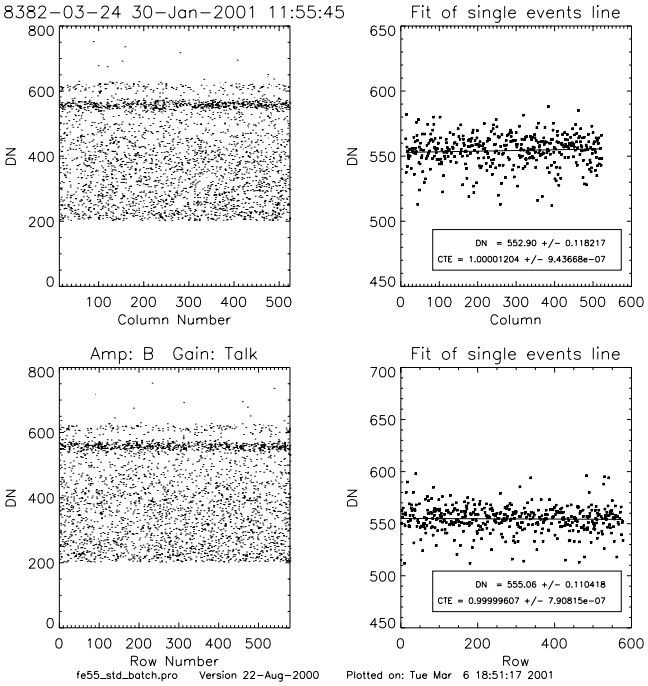

Figure 6. ^{55}Fe "dotplots" indicating parallel and serial CTE measures. Events close to the noise peak have been eliminated for clarity. The right hand plots show linear fits to the data and the derived CTE/pixel. Note that the errors are underestimated and the number of transfers (∼ 500-600) does not allow determination of CTE to levels much above 0.99999

the multiple model curves. These results suggest a back surface that is not completely passivated, yet the back surface implant, anneal and other treatment does provide substantially better QE than that obtained roughly a decade ago with experimental devices fabricated by Tektronix(now SITe) and LMSAL.[13] A subsequent study of the stability of response to very soft X-rays (using Be K at 114 Å) in vacuum indicated < 1% change over an 12 hour period. (Figure 10).

5.2. X-ray Flat Field

X-ray flat fields were obtained by illuminating the CCD using a Manson X-ray source with a carbon target. A pulse-height spectrum taken with a proportional counter verified the beam purity. A series of independent images were added to improve photon statistics (see caption), and the resulting C K X-ray flat field is shown in Figure 11.

5.3. X-ray Spatial Response

As discussed previously, the spatial response of the CCD due to charge diffusion, is an important factor in the overall SXI instrument response. Thus, each flight CCD's X-ray spatial resolution was characterized by the MCC method described in § 3.2. Results of MCC testing are shown in graphical form in Figures 12 and 13. These confirm earlier results shown in Figure 4.

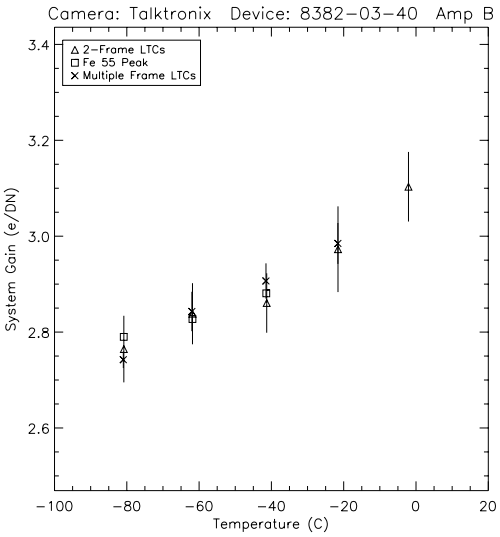

Figure 7. Comparison of CCD + Talktronics system gain measurements. In general the three methods (see text) of determining overall system gain agreed to within 5%.

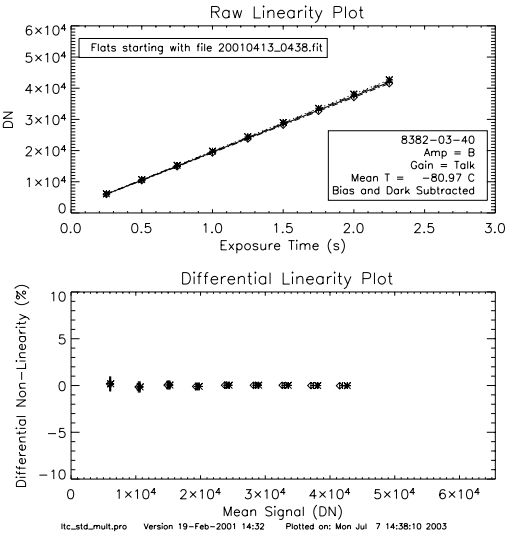

Figure 8. CCD + Talktronics non-linearity as a function of signal. System non-linearity was determined by measuring CCD response at a series of exposure times with an accurate shutter. As can be seen, the linearity of the CCD + test system was better than $\sim 1\%$ over the dynamic range of the CCD.

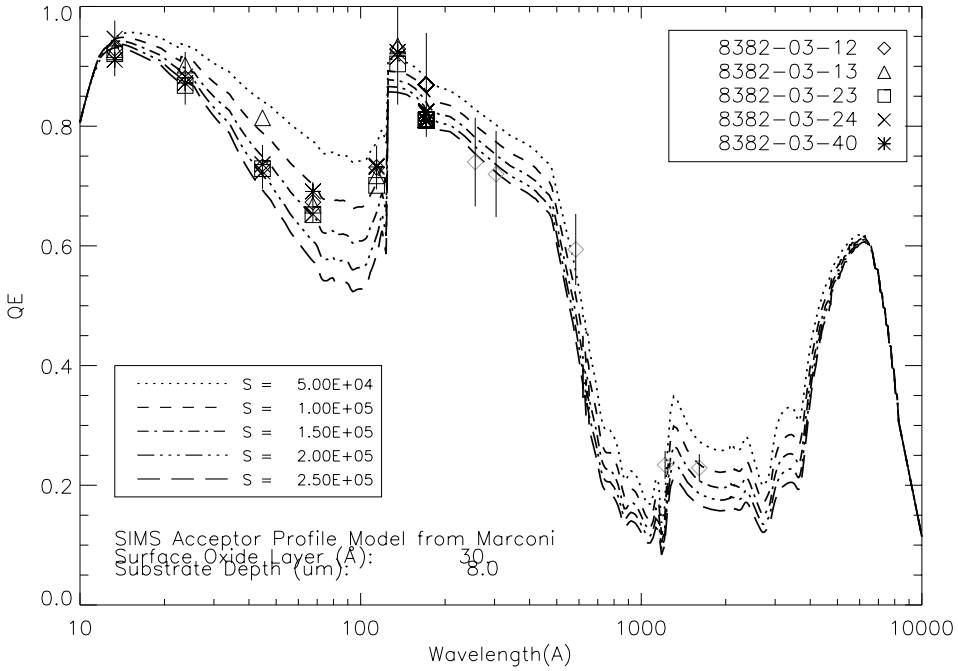

Figure 9. QE Model and Data. Data points are indicated by their CCD S/N. The different curves correspond to changing the S parameter (see text) in the charge collection model.

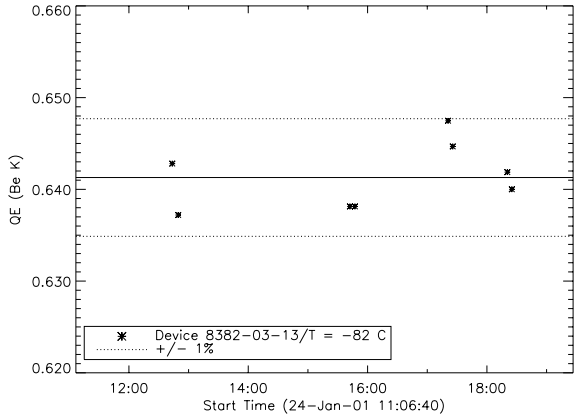

Figure 10. QE stability test over a 12 hour period in vacuum (see text). Dotted lines refer to ±1% variation in QE (of same order as statistical measurement uncertainties).

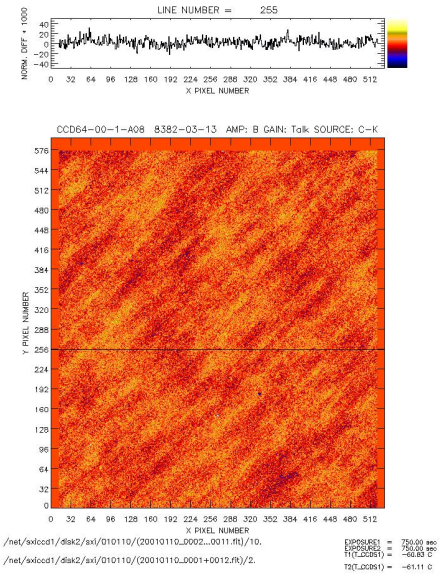

Figure 11. C K (44.7 Å) Flat field made from adding 10 exposures. Diagonal striping at $< 1\%$ level is from anneal process. Random noise in image is dominated by photon counting noise: ~ 77 e^--h pairs/ C K photon results in $\lesssim$ 1000 photons counted per half-full well image. Adding 10 images reduces photon noise to $\sim$ the 1% level.

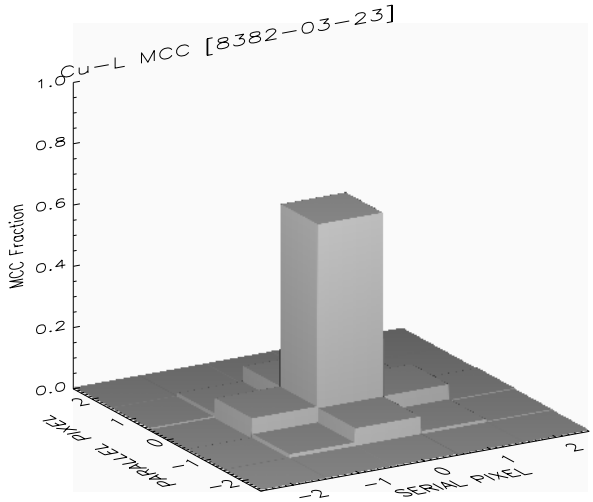

Figure 12. Cu L ((0.93 keV) single photon PSF. MCC is 0.65 for central pixel.

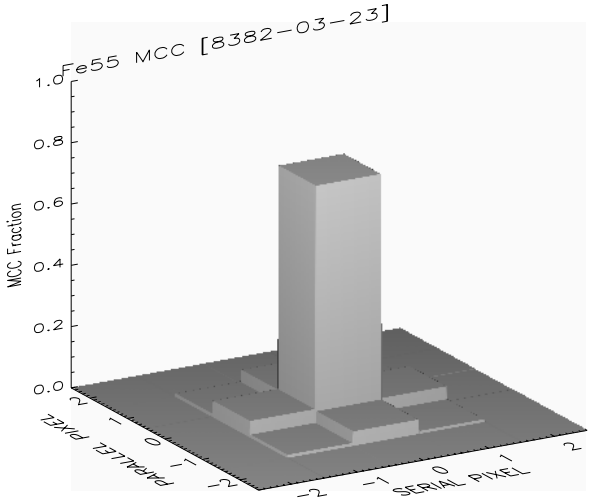

Figure 13. ^{55}Fe (5.9 keV) single photon PSF. MCC is 0.78 for central pixel.

6. RADIATION TESTING

SXI will be in a geosynchronous orbit, and, although the CCD camera head was designed with as much shielding as practicable,[4] the CCD will be subject to proton radiation damage from solar particle events over the course of its operational lifetime.[14] Since such radiation damage is known to cause CTE degradation, especially at low signal levels (e.g Refs. 15,16), we performed radiation testing on a non-flight SXI CCD from the same batch as the flight devices.

6.1. Test conditions and procedure

Device 8382-03-38 was taken to the Harvard Cyclotron facility in an aluminum fixture designed to protect it from ESD damage. The device was masked off so that only a portion of the array received a radiation exposure. The expected SXI proton dose was calculated using a model of the estimated shielding surrounding the SXI CCD ($\sim$ 25 mm Al equivalent), and assuming the solar particle event spectra given in Ref. 14 for N=5 extremely large (EL) proton events (95% confidence for N$\leq$5 over the SXI mission life). Since the cyclotron is a monochromatic source, total expected fluence was corrected using the NIEL (Non-Ionizing Energy Loss[15]) model. The total fluence (2×10^9 p cm^{-2} at 40 MeV) was chosen to represent $\sim \frac{1}{3}$ of this spectrum-weighted fluence, as representative of a "typical" mission with only 1–2 EL events.

6.2. CTE results

The results of the proton irradiation are shown in Figures 14 and 15. The CTE results are generally in agreement with past testing on similar CCDs.[16] We note, however, that these results represent a worst-case scenario for a CCD with a largely empty image area; in the case of the SXI images, which will have a full solar disk imaged over most of the CCD to $\sim$ 50% of full-well, we expect that the actual CTE degradation seen during operations will be much less because of the filling of traps from the first few lines of the solar image (see, e.g. Refs. 15,17).

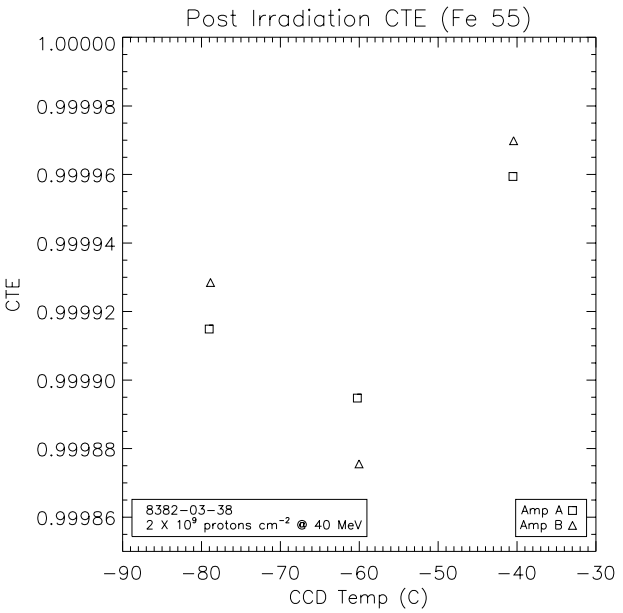

Figure 14. Post Irradiation CTE as a function of temperature

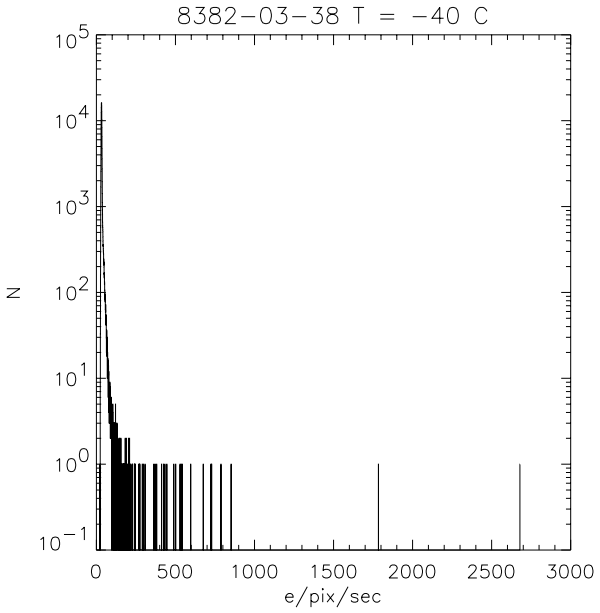

Figure 15. Histogram of dark current distribution post-irradiation

6.3. Dark Spikes

As expected, the proton irradiation also produced a number of pixels with substantially higher dark current than average. These "hot pixels" or "dark spikes", as they are known, have a distribution which is a strong function of temperature.[15] Mitigation of the effects of dark spikes is possible through lowering the CCD temperature and/or annealing the device at room-temperature or higher.[18] Since the SXI CCD temperature is constrained by spacecraft and orbital parameters,[4] we are planning to warm up the SXI CCD periodically (probably during "eclipse season"[4]) to reduce the number and dark rate of these pixels. The dark current generation rate spectrum resulting from the proton irradiation is shown in Figure 15 at -40 C (near the hottest end of the expected SXI CCD temperature operating range). Even in this extreme case, our results indicate that we should expect $<$ 0.1% of all pixels to have a dark current $\gtrsim$ 200 e^- $pixel^{-1}$ sec^{-1} at -40 C by the end of the SXI operational lifetime (assuming the same worst case - 5 EL events - scenario as described above). Since typical exposures for

SXI are $\lesssim$1 s, the effects of such dark spikes can be largely eliminated by the taking of a dark frame of the same length within a reasonable time interval (minutes to hours) of the X-ray image.

7. SUMMARY

A summary of the SXI CCD64 requirements and measured characteristics is given in Table 1. Overall, the performance of the CCD64 devices met or exceeded specifications. The properties of all the flight CCDs were quite similar on a statistical basis. A goal of $> 80\%$ MCC for soft X-rays was nearly achieved by using a thinner (8 μm) device with a matching lower resistivity. The MCC achieved was ultimately limited by fundamental device physics and a stringent requirement on the number of point defects, which would have increased significantly for a back-illuminated device over-thinned beyond the field-free region. Radiation effects due to either charged particles or solar X-ray radiation will degrade the performance of the SXI devices, but only in a gradual fashion, and will not significantly compromise the ability of SXI to meet its operational requirements. Finally, we should note that the successful outcome of the SXI CCD flight development process was due in no small measure to the high degree of communication and cooperative approach taken by all parties.

	SOW requirement	LMSAL Measurement	Notes
Full well	> 100,000 e	> 140,000 e	
Read Noise	< 20 e at -40 C	< 15 e at -40 C	Marconi < 10 e
Charge Transfer Efficiency	> 0.99999	> 0.99999	Measurement accuracy limited
Dark Current	< 4 nAcm-2 at +20 C	< 2 nAcm-2 at +20C equiv	
Linearity	<+/- 3%	<1%	Limited by camera - Marconi is < 1%
Amplifier Gain Stability	2%/ degree C	~0.1%/deg C	agrees with Marconi
X-Ray Quantum Effciency at 44.7 A	50%	65-70%	
X-Ray QE Stability	5%/24 hours	<1% over 6 hours	
X-Ray MCC (Goal) at 44.7 A	80%	65-70% at 13.3 A	Modeling implies 44.7 A will be similar
X-Ray Response Uniformity	correctable to <5% at 5500 A	actual <1% at 44.7, 13.3 A	

Table 1. Summary of CCD64 requirements and measured characteristics

ACKNOWLEDGMENTS

This work was supported by NASA contract NAS5-97181 and the Lockheed Martin Independent Research Program. The authors would like to thank Henry Hancock, Frank Zele, and John Hawley (LMSAL) for their important contributions to the SXI CCD evaluation and flight CCD screening program. Greg Berthiaume (MIT/LL) kindly arranged for proton tests to be run at the Harvard Cyclotron; these tests were developed and conducted by Lori Kahn (Lockheed Martin). Frank Friedlaender (LMSAL) provided a crucial oversight role for the MSSL/Marconi collaboration. Ed McFeaters (LMSAL) and Tony Dibbens (MSSL) were responsible for QA, and much more. We would also like to thank Dave Burrows and Leisa Townsley, of Penn State University, for providing very useful models of CCD spatial response and bringing considerable expertise to discussions at our regular progress meetings.

REFERENCES

1. P. L. Bornmann, D. Speich, J. Hirman, V. J. Pizzo, R. Grubb, C. Balch, and G. Heckman, "GOES solar x-ray imager: overview and operational goals," in *Proc. SPIE Vol. 2812, GOES-8 and Beyond, Edward R. Washwell; Ed.*, pp. 309–319, Oct. 1996.
2. S. Hill and V. J. Pizzo, "Advanced solar imaging from the GOES-R spacecraft," in *Proc. SPIE, Vol. 4853, Innovative Telescopes and Instrumentation for Solar Astrophysics. Edited by Stephen L. Keil, Sergey V. Avakyan*, pp. 465–478, Feb. 2003.

3. M. E. Bruner, R. C. Catura, J. E. Harvey, P. L. Thompson, and P. B. Reid, "Design and performance predictions for the GOES SXI telescope," in *Proc. SPIE Vol. 3442, Missions to the Sun II, Clarence M. Korendyke; Ed.*, pp. 192–202, Nov. 1998.
4. J. R. Lemen and the SXI Team, "Solar x-ray imager for GOES," in *Proc. SPIE Vol. 5171*, p. tbd, 2003.
5. L. Shing, R. A. Stern, P. Catura, M. D. Morrison, T. Eaton, and P. J. Pool, "CCD development and characterization for the GOES N and O Solar X-ray Imager," in *Proc. SPIE Vol. 3765, EUV, X-Ray, and Gamma-Ray Instrumentation for Astronomy X, Oswald H. Siegmund; Kathryn A. Flanagan; Eds.*, pp. 299–309, Oct. 1999.
6. J.-P. Delaboudiniere, G. E. Artzner, J. Brunaud, A. H. Gabriel, J. F. Hochedez, F. Millier, X. Y. Song, B. Au, K. P. Dere, R. A. Howard, R. Kreplin, D. J. Michels, J. D. Moses, J. M. Defise, C. Jamar, P. Rochus, J. P. Chauvineau, J. P. Marioge, R. C. Catura, J. R. Lemen, L. Shing, R. A. Stern, J. B. Gurman, W. M. Neupert, A. Maucherat, F. Clette, P. Cugnon, and E. L. van Dessel, "EIT: Extreme-Ultraviolet Imaging Telescope for the SOHO Mission," Solar Phys. **162**, pp. 291–312, 1995.
7. G. P. Garmire, M. W. Bautz, P. G. Ford, J. A. Nousek, and G. R. Ricker, "Advanced CCD imaging spectrometer (ACIS) instrument on the Chandra X-ray Observatory," in *Proc. SPIE, Vol. 4851, X-Ray and Gamma-Ray Telescopes and Instruments for Astronomy. Edited by Joachim E. Truemper, Harvey D. Tananbaum.*, pp. 28–44, Mar. 2003.
8. L. K. Townsley, P. S. Broos, G. P. Garmire, and J. A. Nousek, "Mitigating Charge Transfer Inefficiency in the Chandra X-Ray Observatory Advanced CCD Imaging Spectrometer," ApJ **534**, pp. L139–L142, May 2000.
9. L. Shing and R. A. Stern, "Development of a low contamination camera head for the evaluation of CCDs in the UV and EUV," in *Proc. SPIE Vol. 1344, EUV, X-ray, and Gamma-ray instrumentation for astronomy*, pp. 396–401, Nov. 1990.
10. S. L. Freeland and B. N. Handy, "Data Analysis with the SolarSoft System," Solar Phys. **182**, pp. 497–500, Oct. 1998.
11. D. Walton, J. L. Culhane, R. A. Stern, and R. C. Catura, "Deep-depletion CCDs for X-ray astronomy," in *Proc. SPIE Vol. 501, State-of-the-art imaging arrays and their applications*, pp. 306–316, 1984.
12. D. L. Windt and R. C. Catura, "Multilayer Characterization at LPARL," in *Proc. SPIE Vol. 984, X-ray multilayers for diffractometers, monochromators, and spectrometers;*, pp. 132–139, 1988.
13. R. A. Stern, L. Shing, and M. M. Blouke, "Quantum efficiency measurements and modeling of ion-implanted, laser annealed charge-coupled devices: x-ray, extreme-ultraviolet, ultraviolet and optical data," Appl.Optics **33**, pp. 2521–2533, 1994.
14. E. G. Stassinopolous, J. L. Barth, and D. W. Nakamura, "Charged Particle Radiation Exposure of Geostationary Orbits for the GOES N,O,P,Q Satellite Program," Tech. Rep. X-900-97-004, NASA Goddard Space Flight Center, 1997.
15. G. R. Hopkinson, C. J. Dale, and P. W. Marshall, "Proton Effects in Charge Coupled Devices," *IEEE Transactions on Nuclear Science* **43**, pp. 614–627, 1996.
16. I. Zayer, I. Chapman, D. W. Duncan, G. A. Kelly, and K. E. Mitchell, "Results from proton damage tests on the Michelson Doppler Imager CCD for SOHO," in *Proc. SPIE Vol. 1900, Charge-Coupled Devices and Solid State Optical Sensors III, Morley M. Blouke; Ed.*, pp. 97–107, July 1993.
17. K. C. Gendreau, *X-Ray Ccds for Space Applications: Calibration, Radiation Hardness, and Use for Measuring the Spectrum of the Cosmic X-Ray Background*. PhD thesis, M.I.T., Jan. 1995.
18. R. A. Kimble, P. Goudfrooij, and R. L. Gilliland, "Radiation damage effects on the CCD detector of the space telescope imaging spectrograph," in *Proc. SPIE Vol. 4013, UV, Optical, and IR Space Telescopes and Instruments, James B. Breckinridge; Peter Jakobsen; Eds.*, pp. 532–544, July 2000.